

## Article

# An Experimental Study on Secondary Transfer Performances of Prestress after Anchoring Failure of Steel Wire Strands

Rihua Yang <sup>1,2,3</sup>, Yiming Yang <sup>1,\*</sup>, Xuhui Zhang <sup>4</sup> and Xinzhong Wang <sup>1</sup>

- <sup>1</sup> School of Civil Engineering, Hunan City University, Yiyang 413000, China; yangrihua@hncu.edu.cn (R.Y.)  
<sup>2</sup> Hunan Engineering Research Center of Development and Application of Ceramsite Concrete Technology, Hunan City University, Yiyang 413000, China  
<sup>3</sup> Key Laboratory of Green Building and Intelligent Construction in Higher Educational Institutions of Hunan Province, Hunan City University, Yiyang 413000, China  
<sup>4</sup> School of Civil Engineering and Mechanics, Xiangtan University, Xiangtan 411105, China  
\* Correspondence: yangyiming@hncu.edu.cn

**Abstract:** To understand the secondary transfer performances of residual prestress after the anchoring failure of end-anchored steel wire strands due to corrosion fracture, six steel wire strand components of post-tensioning prestress were designed and fabricated. One-side fast corrosion was applied to the steel wire strand components using the electrochemical method until anchoring failure was reached. The sphere of influence, stress changes, and the retraction and swelling effect of broken beams after failure were investigated. The influences of factors such as concrete strength, stirrup area, and the length of the component on the secondary transfer length of residual prestress were discussed. Based on the deformation relationship between prestressed steel wire strands and concrete in the stress transfer zone, a stress equation was established and solved through a bond constitutive model. A prediction model of the effective stress transfer length of prestressed steel wire strand after failure was proposed. The results demonstrated that residual prestress can have a secondary transfer after the corrosion fracture of end-anchored steel wire strands, but some effective prestress may be lost. Moreover, the loss of prestress is inversely proportional to concrete compressive strength. When the specimens are relatively short, the prestress loss increases significantly. Concrete strength has significant influences on the length of secondary transfer. The proposed simplified calculation method of the secondary transfer length of residual prestress has a relatively high accuracy, with an average error of 2.9% and a maximum error of 5.2%.

**Keywords:** bridge construction; anchoring failure; residual prestress; secondary transfer; experimental study



**Citation:** Yang, R.; Yang, Y.; Zhang, X.; Wang, X. An Experimental Study on Secondary Transfer Performances of Prestress after Anchoring Failure of Steel Wire Strands. *Metals* **2023**, *13*, 1489. <https://doi.org/10.3390/met13081489>

Academic Editors: Cemal Basaran and Janice Barton

Received: 29 June 2023

Revised: 28 July 2023

Accepted: 17 August 2023

Published: 18 August 2023



**Copyright:** © 2023 by the authors. Licensee MDPI, Basel, Switzerland. This article is an open access article distributed under the terms and conditions of the Creative Commons Attribution (CC BY) license (<https://creativecommons.org/licenses/by/4.0/>).

## 1. Introduction

Due to its good durability, mature construction technology and prestressed concrete structures have been extensively applied in bridge engineering [1–4]. The effective transfer of prestress to concrete is the basic condition for the normal operation of prestressed structures. In general, the post-tensioned members complete the transfer of prestress through the anchorage and the plate under the anchorage, while the pre-tensioned members complete the transfer of prestress through the bond between the prestressed reinforcement and the concrete [5]. The length from the end surface of prestressed tendons with zero stress to the end surface with effective prestress in the pre-tensioning components is called the transfer length of the prestressed tendons [6]. Hence, there are two key factors that influence the transfer length of prestress. One is the bond force, and the other is the Hoyer effect [7,8]. When the prestressed tendons are swelled or develop rust fractures, the retraction diameter at the end increases to form a wedge-shaped effect. Therefore, accurately determining the prestress transfer length is crucial to bridge structural design and structural safety.

At present, many studies on prestress transfer length based on the pre-tensioning method have been published. Moreover, the calculation formula of transfer length has been provided in the standards of many countries [9–12]. Some scholars have carried out experimental and theoretical studies on prestress length and compared their results with the transfer length determined by the standard calculation method. They believe that the calculation of prestress transfer length in standards is too conservative and safe [13–15]. Some scholars have studied key factors that influence transfer length, and they believe that factors such as concrete strength, corrosion, the concrete cover, and circumferential constraints as well as the shape and diameter of rebars can influence the prestress transfer length [16–18]. Among the above factors, concrete strength is accepted as a main influencing factor of transfer length. A higher concrete strength is accompanied by a lower bond length. However, some studies believe that when the concrete strength is higher than 55 MPa, the bond length may not decrease with the increase in concrete strength [19,20]. Moreover, the transfer length increases with the increase in the corrosion rate of prestressed tendons. The provision of a circumferentially constrained spring-loop around the strand can significantly shorten the prestressed transfer length (an approximately 45% reduction) and can effectively improve the stress condition of the beams [21]. When the concrete cover is less than 5.5 times the diameter of the steel strand, the smaller cover thickness will result in a longer transfer length. However, when the concrete cover exceeds 5.5 times the diameter of the steel strand, it becomes challenging for the prestressed steel strand to undergo splitting failure during the transfer process. In this case, further increasing the cover thickness has a less significant impact on the transfer length [19]. Hence, the transfer length is not obviously influenced if the thickness of the concrete protective cover continues to increase [22]. Moreover, the prestress transfer length increases with the increase in the corrosion rate [23].

Nevertheless, existing studies are mainly based on pre-tensioning components. The corrosion of steel wire strands is not obvious in the early period due to the protection of prestressed pipelines. However, with the increase in the service years of components, many construction defects appear, such as insufficient grouting and delayed sealing anchoring of the end anchoring zone. Under the coupling effect of high stress and the environment, prestressed tendons not only have electrochemical corrosion similar to ordinary steel bars, but may also have several forms of hydrogen embrittlement, stress corrosion, and crevice corrosion. As a result, the prestressed tendons may develop brittle fracture when the prestress is far lower than the yielding strength [24]. The prestress which is lost at prestressed beam end after anchoring failure can be transferred again through bonding. The mechanism is similar to pre-tensioned prestressed tendons, but there are still some differences. On the one hand, post-tensioned rebars are built in a dense arrangement, thus making the Hall effect more significant [25]. On the other hand, the corrosion of prestressed beams progresses slowly, which is different from the fast expansion of pre-tensioned rebars. Moreover, differences in bond force may also influence the transfer of stresses.

Secondary transfer of residual prestress and anchoring after the stress fracture of prestressed beams have been studied preliminarily [26]. In experiments, specimens were reinforced by replacing ribbed steel tubes with corrugated pipes. The results demonstrated that the prestressed beams can achieve a second anchoring through the bonding of press mortar after anchoring failure. Additionally, the bending strength of species after the local fracture of steel wire strands has been investigated, and it was found that the bending capacity of components with end anchoring failure decreased by only 7.2% [27,28]. Nevertheless, the calculation and evaluation methods of the secondary transfer length of residual prestress have not yet been reported in existing studies. Systematic studies on stress transfer after fracture failure of the end anchoring of prestressed beams are still lacking.

In this study, an anchoring failure experiment at unilateral strand ends of six post-tensioning prestressed concrete specimens was carried out. Based on the experimental results, the secondary transfer behaviors of residual prestress in prestressed tendons after fracture were analyzed. The influences of concrete strength and stirrup configuration on

the secondary transfer performances of residual prestress were discussed. The calculation method of the secondary transfer length of residual prestress after the fracture of the end prestressed strands was proposed based on concrete compressive strength.

## 2. Experiment

### 2.1. Specimen Design

A total of 6 post-tensioning PC specimens were designed and fabricated in this experiment, which were numbered as S1–S6. Cross-section dimensions of all drawing specimens were 300 mm × 500 mm. The detailed sizes of specimens are shown in Table 1.

**Table 1.** Parameters of specimens S1–S6.

Specimens	Cross-Section Dimension/mm	Length/mm	Concrete Mark	Stirrup Diameter
S1	300 × 500	1000	C50	Φ8
S2	300 × 500	1250	C50	Φ8
S3	300 × 500	1000	C40	Φ8
S4	300 × 500	1000	C60	Φ8
S5	300 × 500	1000	C50	Φ10
S6	300 × 500	1000	C50	Φ12

A corrugated pipe with a diameter of 60 mm was reversed in the center of specimens. Three seven-wire prestressed strands with a diameter of 15.2 mm and a strength grade of 1860 MPa were designed in the corrugated pipe. A total of 8 pieces of Φ12 mm HRB400 deformed bars were arranged longitudinally out of the corrugated pipe. The stirrups were arranged along the length direction of the specimen with a spacing of 100 mm. To study the influences of concrete strength and the stirrup reinforcement ratio on stress transfer and anchoring performances of the prestressed beam after failure, three concrete strength grades (C40, C50 and C60) and three stirrup configuration forms (Φ8@100 mm, Φ10@100 mm and Φ12@100 mm) were designed for the specimens. The stirrup model used HPB235 plain round bars. The reinforcement layout of the specimens is shown in Figure 1.

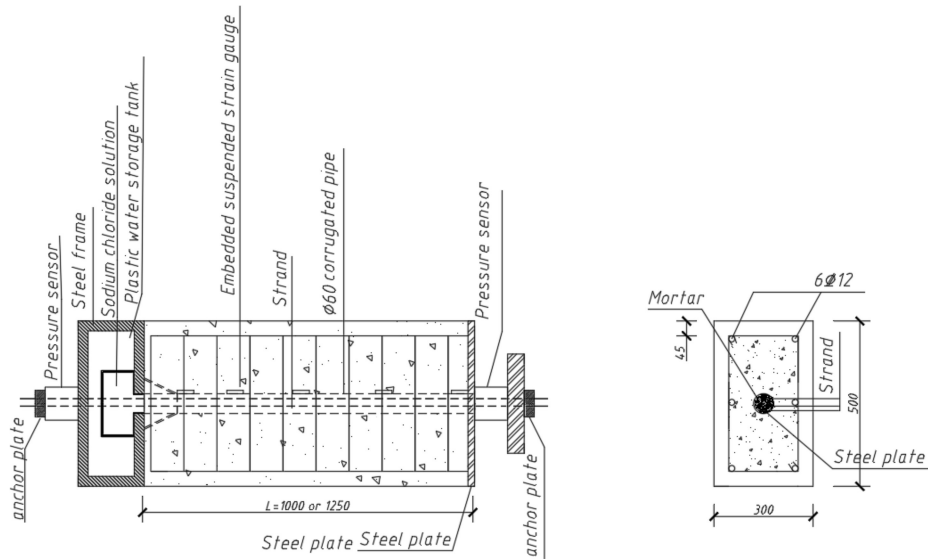


**Figure 1.** Dimensions and reinforcement of S1–S5 (unit: mm).

The tension control stress of the steel wire strand is 1395 MPa, which is 0.75 times that of the standard tensile strength of the strand. The material properties of steel wire strands and ordinary steel bars are listed in Table 2. The concrete applied was the 42.5 ordinary Portland cement, and natural river sand was used as the fine aggregate. The coarse aggregate used graded broken stones, and the maximum nominal particle size was 25 mm.

Tap water in the laboratory was used for stirring and mixing the materials. The mixing ratio of C40 concrete was determined as cement/sand/stone/water = 1:1.33:2.82:0.42. The mixing ratio of C50 concrete was cement/sand/stone/water = 1:1.62:2.73:0.44. The mixing ratio of C60 concrete was cement/sand/stone/water = 1:1.59:3.15:0.44. The commercial cement paste with the same grade of concrete was applied as the mortar. The same batch of concrete was collected and prepared into cubic standard specimens and cured together with test components. The average 28 days compressive strengths of C50, C40, and C60 concrete specimens were 53.5 MPa, 42.6 MPa, and 63.3 MPa, respectively.

**Table 2.** Material properties of steel wire strand and ordinary steel bars.

Diameter (mm)	Yield Strength (MPa)	Ultimate Strength (MPa)	Elasticity Modulus (GPa)	Elongation Rate (%)
15.2	1860	1915	195	14.3
12	476	612	200	14.5
8	263	366	210	15.3
10	285	357	210	18.2

## 2.2. Layout of Strain Gauges

Since the test steel wire strand was twisted with 7 wires, there was a twist angle. It is impossible to make axial notches on the steel wire strand or to paste strain gauges on the surface to monitor the strains of the strand. Hence, suspension strain gauges were set on the external wall of corrugated pipes at an interval of 17.5 cm to monitor the strains of the concretes. The suspension method of the embedded strain gauge is as follows: firstly, a larger-diameter corrugated pipe is used, and a steel plate is set below the anchor during the production of specimens. Subsequently, near the vicinity of the corrugated tube, an ordinary reinforcement along the length direction of the specimen is welded from both sides of the steel plate. Finally, the embedded strain gauge is securely fastened by tying it to the ordinary reinforcement using steel wires. On this basis, the strain distribution and real-time bond length of the steel wire strand were estimated. The distribution of the strain gauges is shown in Figure 2.

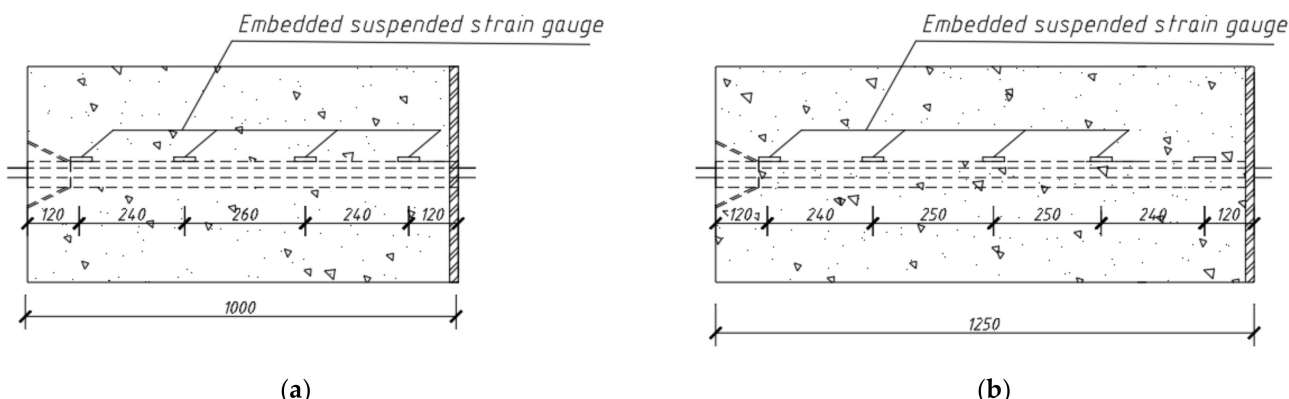


**Figure 2.** Layout of strain gauges in S1–S6 (unit: mm): (a) S1, S3–S6; (b) S2.

## 2.3. Tension and Effective Prestress of Prestressed Tendons

The tension control stress of prestressed tendons was 1395 MPa. In the prestressing process, tension force was monitored with a rope meter, and elongation of the steel wire strand was recorded by a dial indicator. At 48 h after tension, the rope meter was read, and effective prestress applied onto components was measured in Table 3.

**Table 3.** Effective prestress in different test stages.

Specimens No.	S1	S2	S3	S4	S5	S6
Tension prestress (kN)	636.12	636.12	636.12	636.12	636.12	636.12
Effective prestress before corrosion test (kN)	497.2	511.3	449.9	510.5	501.1	505.2
Effective prestress after anchoring failure (kN)	434.7	426.3	465.3	445.6	453.3	434.7

#### 2.4. The Fast Corrosion Fracture an End Anchoring Position of Prestressed Tendons

After curing for 28 days after grouting, local corrosion of the end anchoring position of S1–S5 was performed via laboratory fast electrochemical corrosion. In this experiment, a 20 cm long local etch trench was designed, and it was fixed onto the end zone of the concrete component through structural adhesive. The trench contained 5% NaCl solution and a stainless steel plate. An anode wire with constant DC power was connected to the steel wire strand during corrosion, while the cathode wire was connected to the stainless-steel plate in the corrosion trench. Meanwhile, pouring NaCl solution into the trench formed a current loop. Under the action of the current, the steel wire strand at the anode was corroded (Figure 3). Only the corrosion of the strand end was considered during the experiment. To avoid the influence of corrosion on ordinary steel bars, epoxy resin was used as a coating during binding of the framework of the ordinary steel reinforcement for rust prevention. The whole experiment was carried out in an environment with a temperature of 20 °C and a humidity of 65%. The corrosion time of components was about 5 days. According to examination, this was consistent with the experimental design. Prestressed tendons all developed corrosion fracture at the end of the experiment (Figure 4).

**Figure 3.** Corrosion layout of experimental components.**Figure 4.** End anchoring corrosion fracture of test specimens.

### 3. Test Results and Analysis

#### 3.1. Concept of Secondary Transfer of Residual Prestress

The methods to apply prestress onto structures include the pre-tensioning method and the post-tensioning method, as shown in Figure 5. During the pre-tensioning of components, the wedge effect is caused by the Poisson effect during the expansion of the strand under the influence of effective prestress. At the same time, there is internal shrinkage and slip occurring in the steel strand. The above two phenomena lead to the secondary transfer of residual prestress. It is worth noting that since the steel strand's small diameter leads to an inconspicuous wedge effect, the prestress transfer is mainly caused by the bond effect between the concrete and the steel strand.

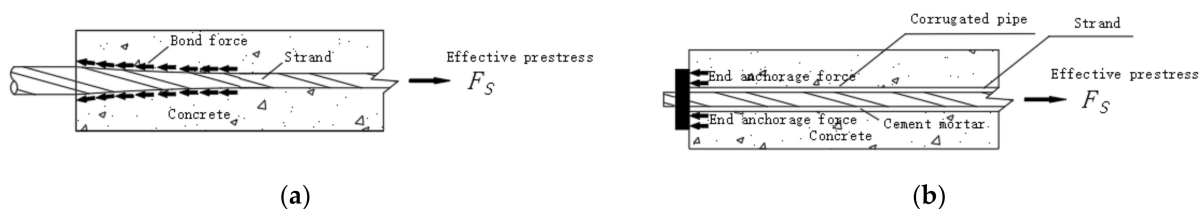


**Figure 5.** Principle of prestress application: (a) pre-tensioning method, (b) post-tensioning method.

For the post-tensioning prestressed components with end corrosion fracture, the stress at the fracture was zero due to the anchoring failure of the anchorage device. If concrete can provide enough bond force, the steel wire strand will generate a wedge effect, which is similar to the pre-tensioning components. Moreover, the steel wire strand will shrink and slip, thus causing the secondary transfer of residual prestress.

#### 3.2. Strain Distribution

After the breakage of the steel wire strand, the secondary transfer of residual prestress is accompanied by stress changes. Hence, stress changes at the fracture side of the steel wire strand specimens when the initial prestress was 100%, 75%, 50% and 25% were examined in this study. The results are shown in Figure 6.

It can be seen from Figure 6 that with the increase in the corrosion rate, strains at the corrosion end of all of the specimens change violently. With the increase in the distance to the corrosion end, the strain decreases quickly. All specimens had the smallest strain changes at the third strain gauge, which tended to be zero. This might be because the good bonding between the steel wire strand and the concrete may lead to the secondary transfer of residual prestress after the fracture of the steel wire strand.

The strain begins to increase at the fourth strain gauge. This demonstrates that prestress can undergo a secondary transfer in specimens after the fracture of the steel wire strand, but the effective prestress may decrease. The reasons for this are analyzed as follows. The end anchor plate and rope meter are both made of steel materials, and their elasticity moduli are far higher than that of concrete. When the strand stress at the corrosion side decreases, the concrete compressive strain in the local corrosion range is released, thus influencing the concrete stress distribution of the components. Due to the different elasticity modules between the concrete and the anchor plate, the relative strain generated by the concrete is higher than that of the anchor plate. To keep the coordination of the displacement between the concrete and the anchoring device at the non-corroded end, the anchor plate moves toward the corrosion end relative to the concrete. The length of the steel wire strand decreases and the effective prestress decreases, while the prestress loss increases.

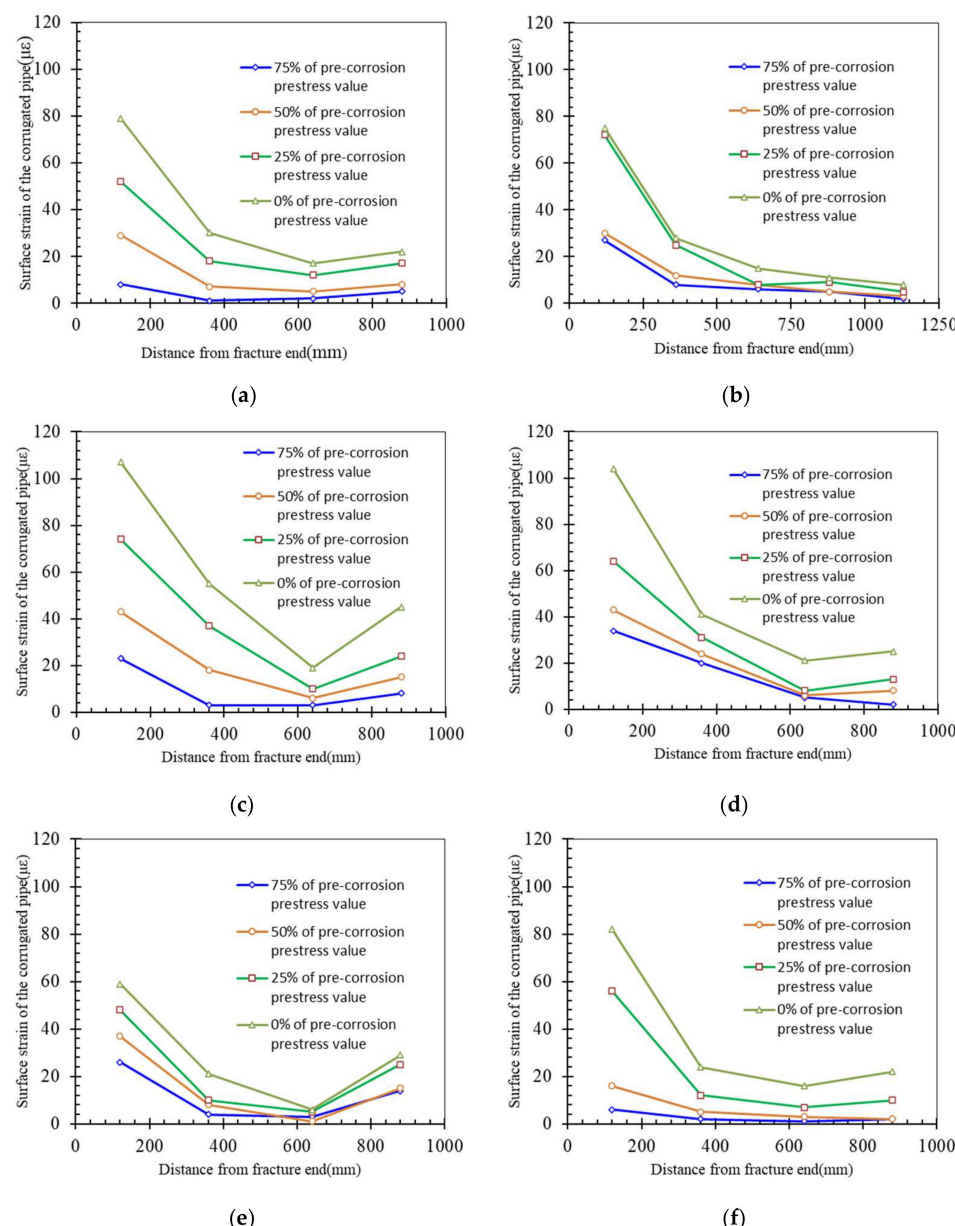


**Figure 6.** Strain distribution of specimens under corrosion state: (a) S1; (b) S2; (c) S3; (d) S4; (e) S5; (f) S6.

### 3.3. Stress Distribution of Rope Meter

It can be seen from Figure 6 that the strain close to the non-corrosion end increases. The tensile strength values read from the rope meter at the non-corrosion end of specimens before and after the corrosion fracture of the steel wire strand are shown in Figure 7. Clearly, the tensile strength values of S1-S6 decreased after the strand fracture occurred at the corrosion end. This further proves that effective prestress may decrease after the secondary transfer.

The effective prestress of S1 at the non-corrosion end decreases by 62.5 kN, showing a loss ratio of 12.6%. It decreases by 86.6 kN in S3, showing a loss ratio of 19.2%. It decreases by 40.2 kN in S4, showing a loss ratio of 7.9%. From the above analysis results, it can be seen that the strength of the concrete has a great influence on the prestress loss. This is mainly due to the fact that concrete with a lower elastic modulus will produce a larger compressive strain under the action of the released anchorage force at the corroded end. This change also leads to larger tensile strains in the anchorage with a larger elastic modulus and the

steel strand according to the principle of displacement coordination, ultimately resulting in a reduction in the effective prestress at the uncorroded end.

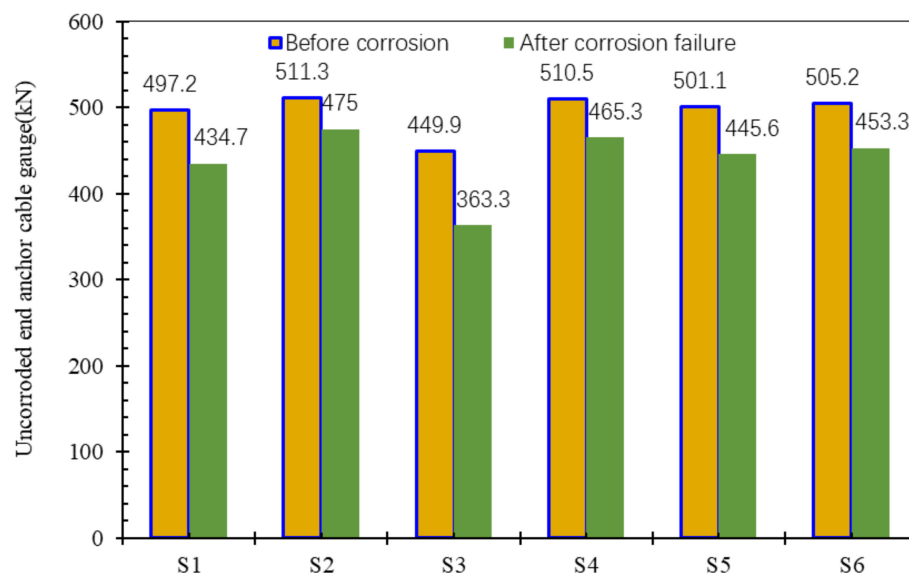


**Figure 7.** Tensile force of rope meters of S1–S6.

All test parameters of S1 and S2 were the same except for the length of component. It can be seen from Figure 8 that effective prestress at the non-corrosion end decreases by 62.5 kN in S1 and 36.3 kN in S2, showing a loss ratio of 7.1%. With the increase in the length of the component, the sphere of influence of the secondary transfer on the concrete at the non-corrosion side decreases. Hence, a smaller relative displacement is generated between the concrete at the non-corrosion side and the anchorage device, thus resulting in a smaller prestress loss.

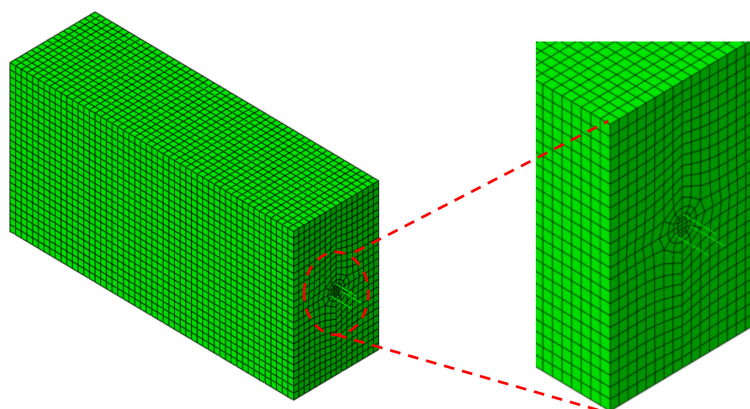


**Figure 8.** Overall structural model.

All test parameters of S1, S5, and S6 were the same, except for the stirrup diameter. It can be seen from Figure 8 that the effective prestress at the non-corrosion end decreases by 62.5 kN in S1 and 55.5 kN in S5, showing a loss ratio of 11.1%. The effective prestress at the non-corrosion end decreases by 51.9 kN in S6, showing a loss ratio of 10.3%. The stirrup reinforcement ratio has no obvious influence on prestress loss. This is because the concrete generally does not develop splitting failure due to the large cross-section size of the specimens in the experiment. The horizontal constraint of the stirrups against the steel wire strand has not been completely developed. Hence, the stirrup reinforcement ratio has a small influence on the effective prestress.

Obviously, the effective prestress decreases after the secondary transfer of residual prestress due to the fracture of the steel wire strand. When the length of the specimens is sufficient, the effective prestress value is relatively sensitive to concrete strength. When the thickness of the concrete protective cover exceeds five times the diameter of the steel wire strand, the stirrup configuration has small influences on the effective prestress of the secondary transfer if the component has no splitting failure.

#### 4. Calculation Method of Secondary Transfer Length

Since the secondary transfer after the fracture of the post-tensioning steel wire strand is similar to that of the pre-tensioning steel wire strand, the steel strand will shrink and slip. As a result, prestress is transferred through bonding slippage between the concrete and the steel strand. According to the definition of pre-tensioning transfer length, the secondary transfer length can be defined as the distance at which the steel wire strand stress increases from 0 to effective prestress after fracture.

##### 4.1. Basic Hypotheses

(1) The thickness of the protective cover of the steel wire strand component is high enough, and the influences of initial prestressed cracks are ignored.

(2) The bond stress is equal in the transfer length range. According to the research results [29], the relationship between the average bond stress ( $\tilde{\tau}$ ) and the maximum bond stress ( $\tau'_{\max}$ ) in the secondary transfer length of residual prestress is:

$$\frac{\tau'_{\max}}{\tilde{\tau}} = 1.25 \quad (1)$$

where  $\tau'_{\max}$  is the maximum bond stress in the transfer length and  $\tilde{\tau}$  is the average bond stress in the transfer length. It is worth noting that the shear stress is assumed to be uniformly distributed along the longitudinal direction of the prestressed reinforcement in order to simplify the calculation.

(3) According to [30], the maximum bond stress of the steel wire strand is:

$$\tau'_{\max} = 2.1 \times \frac{\sqrt{f_c}}{n^{0.64}} \quad (2)$$

where  $f_c$  is the concrete compressive strength and  $f_c = 0.76 f_{cu}$ , and where  $n$  refers to the number of wires in the strand.

(4) The corrugated pipe has good bonding with concrete, showing coordinated and consistent deformation.

##### 4.2. Process Stress Analysis and Calculation of Secondary Transfer Length

According to the equation of equilibrium of forces, there is an equilibrium equation between the bond force in the transfer length and the actual prestress at the beginning of corrosion of the steel wire strand:

$$\tilde{\tau} \sum_s l_t = \sigma_p A_p \quad (3)$$

Bringing Equations (1) and (2) into Equation (3), one obtains:

$$l_t = \frac{\sigma_p A_p n^{0.64}}{1.68 \times \sqrt{f_c} \times \sum_s} \quad (4)$$

where  $\sum_s$  is the perimeter of the steel wire strand,  $l_t$  is the transfer length,  $\sigma_p$  is the actual effective tensile strength of the steel wire strand before corrosion, and  $A_p$  is the area of the steel wire strand.

According to regulations [12], the prestress transfer length of a  $1 \times 7$  steel wire strand was calculated according to the following equation:

$$l_t = 0.17 \frac{\sigma_p}{f'_t} d \quad (5)$$

where  $f'_t$  is the tensile strength of concrete and  $f'_t = 0.26 f_{cu}^{2/3}$ , and where  $d$  is the nominal diameter of a single-wire strand.

The secondary transfer lengths of prestress of S1–S6 were calculated according to Equations (4) and (5). The results are shown in Table 4. It can be seen from Table 4 that the initial prestress of S4 is the lowest, but its transfer length is the highest. Compared to S4, S5 shows higher initial prestress, but the lowest secondary transfer length. This is mainly because concrete strength is an important factor that influences secondary transfer length. The concrete with the greater compressive strength has the higher tensile strength, and the possibility of microcracks in concrete declines. This also determines the stronger bond force between the concrete and the steel wire strand, which needs a smaller transfer length. S5 and S6 had stirrup reinforcement, but this had no obvious influence on secondary transfer length because the prestress in the secondary transfer is insufficient to make the concrete specimens develop splitting failure. The stirrups restrict the development of cracks in the concrete, and the three-way constraint against concrete is not increased obviously. It can be seen from Table 4 that the transfer length in Equation (4) is smaller than that in Equation (5), with an error of 19.3–24.5%. The maximum error is observed in S3. The transfer length in Equation (4) is smaller than the calculated transfer length in the standards, which is related to the relatively conservative and safe calculations found in the standards.

**Table 4.** Secondary transfer length of S1–S6.

Specimen No.	Concrete Compressive Strength/MPa	Tensile Force of the Strand at the Beginning of Corrosion/kN	Transfer Length in Equation (4) $l_{t1}/\text{mm}$	Transfer Length in Equation (5) $l_{t2}/\text{mm}$	Relative Error/%
S1	53.5	497.2	655	839	21.9
S2	53.5	511.3	673	858	21.6
S3	42.6	449.9	664	879	24.5
S4	63.3	510.5	618	766	19.3
S5	53.5	501.1	660	841	21.5
S6	53.5	505.2	665	848	21.6

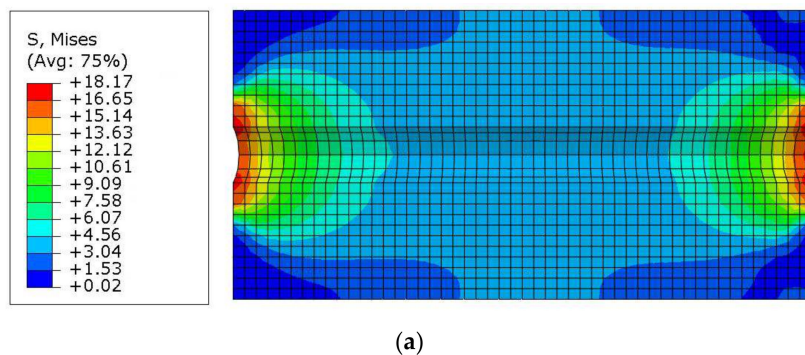
#### 4.3. Numerical Simulation Analysis

A finite element calculation model of the damaged concrete components was constructed using ABAQUS (version of Abaqus CAE2016, Dassault systems, Vélizy-Villacoublay, France). The structure was constructed using the separated model. Concrete was simulated using the reduced integral hexahedral units (C3D8R) and the concrete applied the constitutive damage of plasticity (CDP) [31]. Both ordinary steel bars and prestressed bars were simulated using truss units (T3D2). The double broken line equi-hardening constitutive relation model was chosen. The bond slip between the steel wire strand and the concrete was simulated using the nonlinear spring units (SPRING2), which was realized by setting units parallel and perpendicular to bars at nodes between the concrete and steel wire strand. In the model, there were 28,522 nodes and 25,723 units. It should be noted that in order to more reasonably simulate the local load effects at the end of the beam, a strategy of manually refining the mesh locally was employed. Within a radius of 47.0 mm from the center of the cross section (i.e., around the steel strands), the elements were divided into four smaller elements. These elements had dimensions of 9.5 mm, 9.5 mm, 11.0 mm, and 17.0 mm, respectively, along the radial direction of the steel strands. Except for the above area, the dimensions of all the other units were 20 mm  $\times$  18.75 mm  $\times$  20 mm. The whole model structure is shown in Figure 8.

To simulate the fracture of the steel wire strand, the passivation and activation of units were realized through model changes in the interaction module. Step 1 involves inactivating all units of the structure. Step 2 involves activating the concrete units, anchor bearing plate, steel wire strand, reinforcement cage, and boundary conditions, except the grouting part. Step 3 involves applying prestress through the temperature-falling method. Step 4 involves activating the grouting units. Step 5 is to “passivate” the steel wire strand units and anchor base plate at the fracture position.

To verify the validity of the secondary transfer of residual prestress, the stress distributions in the concrete and steel wire strand when the effective prestress at the corrosion side was 50% and 0% before and during the corrosion in the zone are provided in Figures 9 and 10, respectively. It can be seen from Figure 9 that with the increase in the corrosion rate, the prestress at the concrete corrosion side of the central section of the beam declines slightly, and it is transferred to the non-corrosion end gradually. Obvious shrinkage and slippage with the strand are generated. This can prove that residual prestress can be transferred again. Meanwhile, the prestress distribution in anchor concrete on the non-corrosion side basically remains the same. It can be seen from Figure 10 that the prestress declines sharply with the increase in the corrosion rate. As the distance to the corrosion end increases, the reduction in the effective prestress gradually slows down until it stays basically constant. In this way, the secondary transfer of residual prestress is finished. As the corrosion fracture process is completed, the effective prestress on the non-corrosion side decreases from 1186 MPa to 1165 MPa. Therefore, the residual prestress can undergo secondary transfer after the end of the corrosion fracture, which is similar to the pre-tensioning components. However, the effective prestress will decrease.

Since concrete strength has significant influences on the secondary transfer length of residual prestress, the stress distribution in the concrete and steel wire strand when the initial effective pre-tension values of S1, S3, and S4 are 450 kN was discussed with reference to the design parameters of the beams. The results are shown in Figures 11 and 12. It can be seen from Figure 11 that the secondary transfer length of residual prestress is negatively related with concrete strength. The influences of concrete strength on the anchoring prestressed zone on the corrosion size are decreased obviously. It can be seen from Figure 12 that the secondary transfer length of the residual prestress of S1, S3, and S4 were 650 mm, 700 mm, and 630 mm. With the increase in concrete strength, the stress variation gradient of the steel wire strand on the fracture size is more obvious. A shorter secondary transfer distance is conducive to reaching a basically constant stress of the steel wire strand.



(a)

**Figure 9. Cont.**

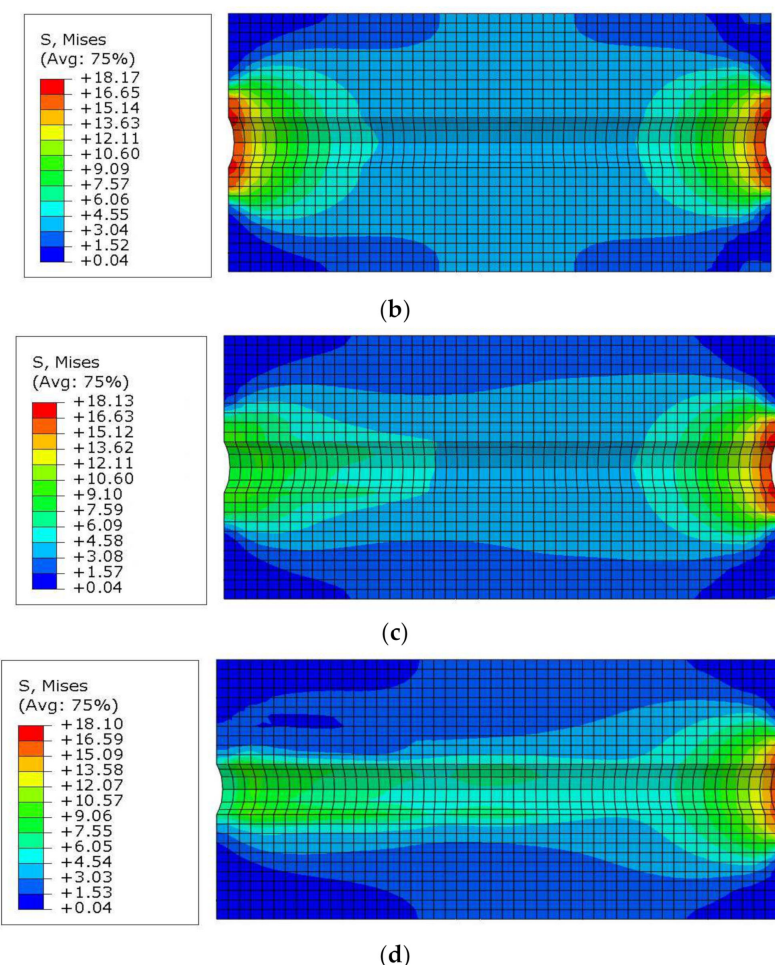


**Figure 9.** Concrete stress distribution of longitudinal middle section of S1 (MPa): (a) Stress distribution of concrete before corrosion of steel strand ( $Fe = 497 \text{ kN}$ ); (b) Effective pre-tension on the corrosion side ( $Fe = 497 \text{ kN}$ ); (c) Effective pre-tension on the corrosion side ( $Fe = 249 \text{ kN}$ ); (d) Effective pre-tension on the corrosion side ( $Fe = 0 \text{ kN}$ ).

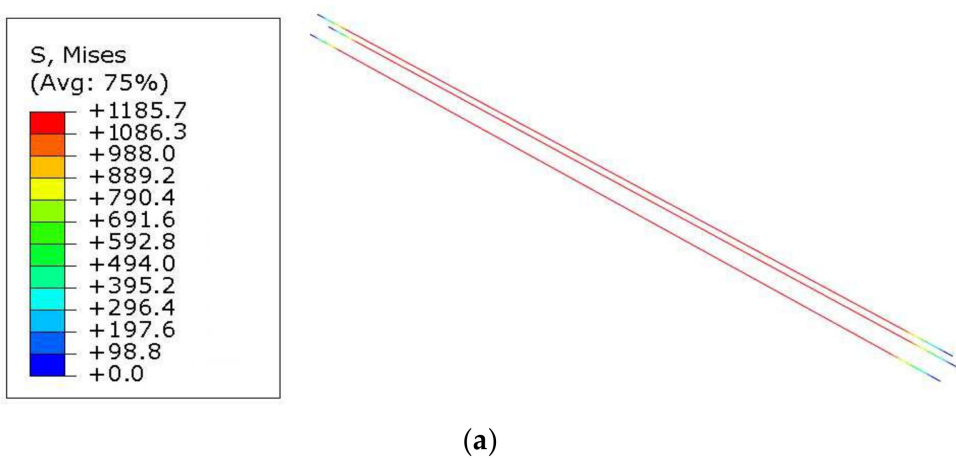


**Figure 10.** Cont.

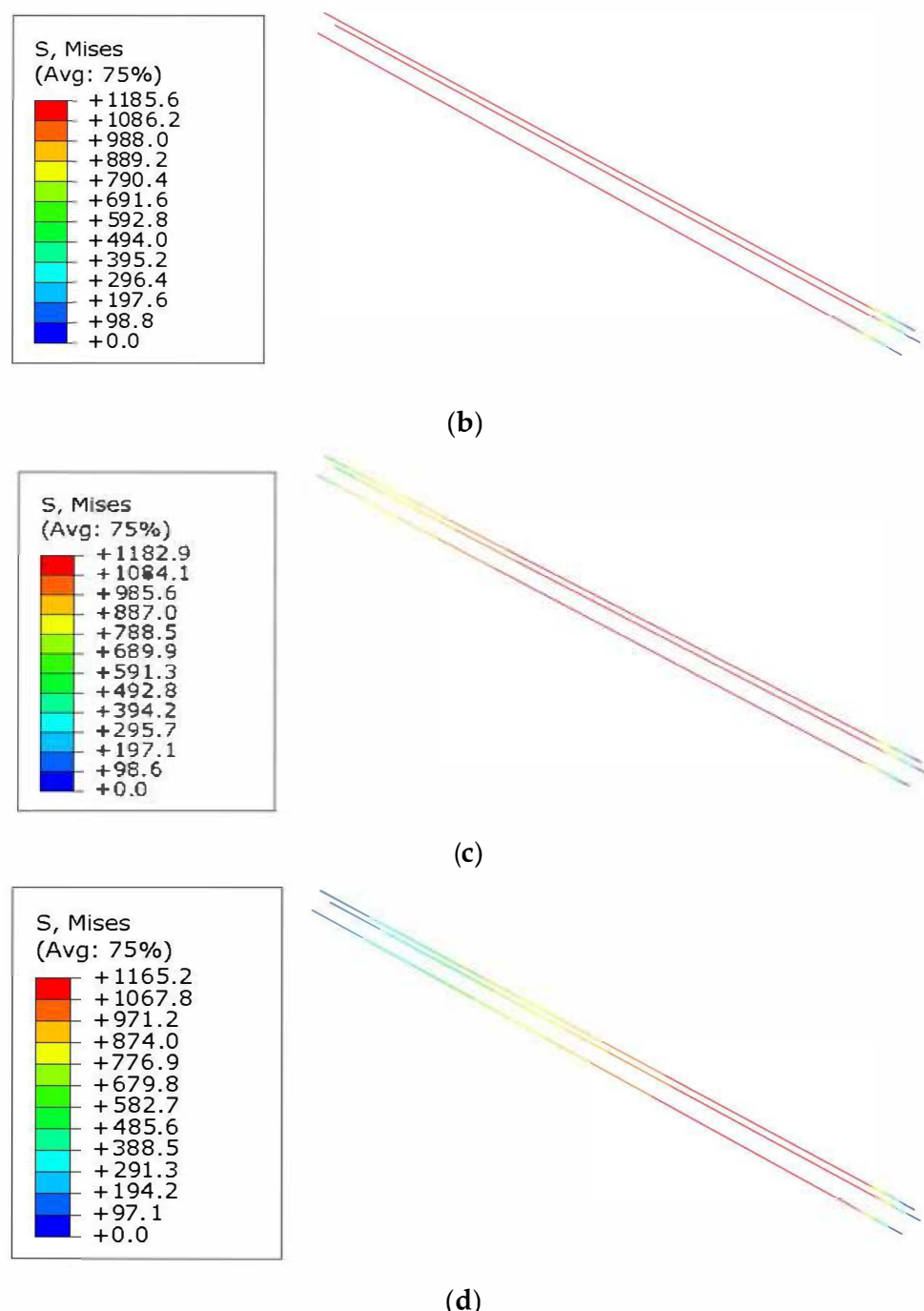


**Figure 10.** Stress distribution of steel wire strand of S1 before and during corrosion (MPa): (a) Stress distribution of prestressing steel strands before corrosion ( $Fe = 497 \text{ kN}$ ); (b) Effective pre-tension on the corrosion side ( $Fe = 497 \text{ kN}$ ); (c) Effective pre-tension on the corrosion side ( $Fe = 249 \text{ kN}$ ); (d) Effective pre-tension on the corrosion side ( $Fe = 0 \text{ kN}$ ).

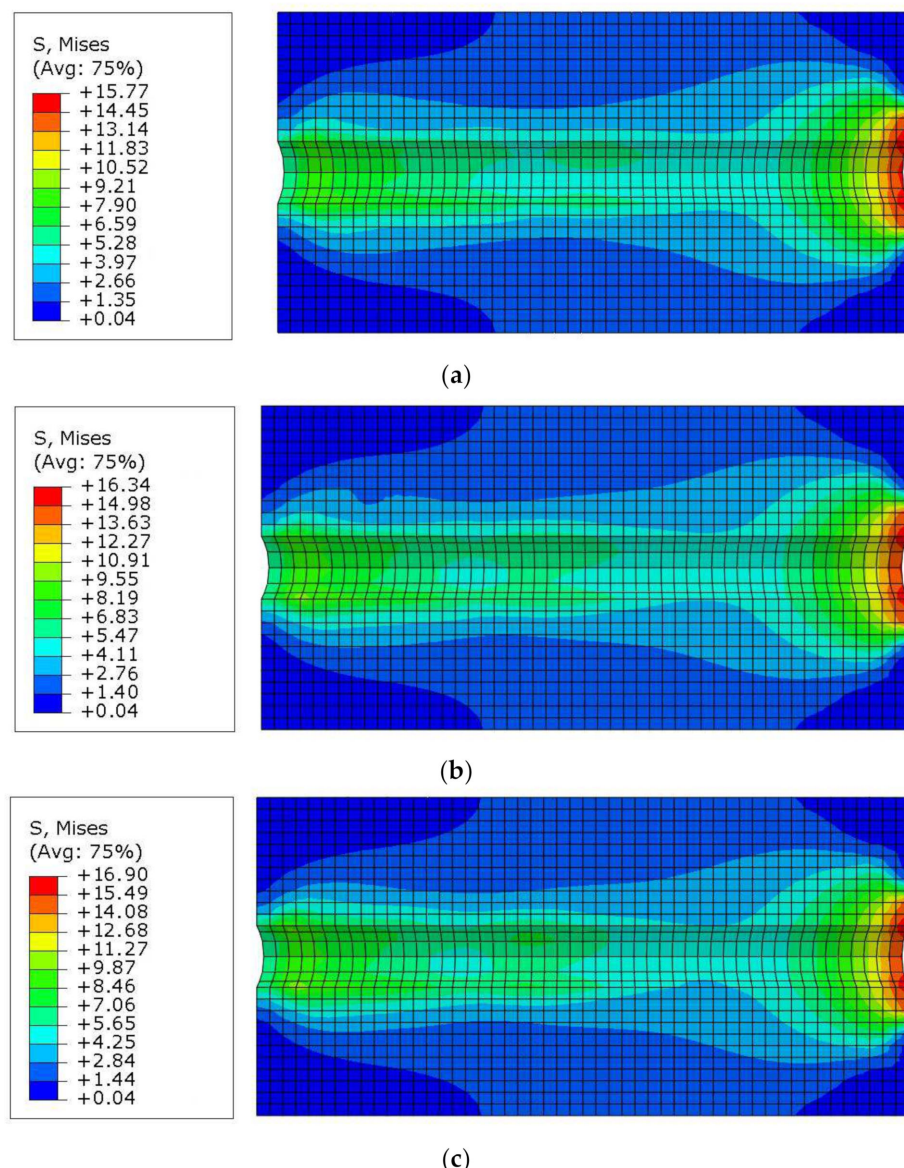


**Figure 11.** Concrete stress distributions at end anchoring failure of one side (MPa): (a) S3; (b) S1; (c) S4.

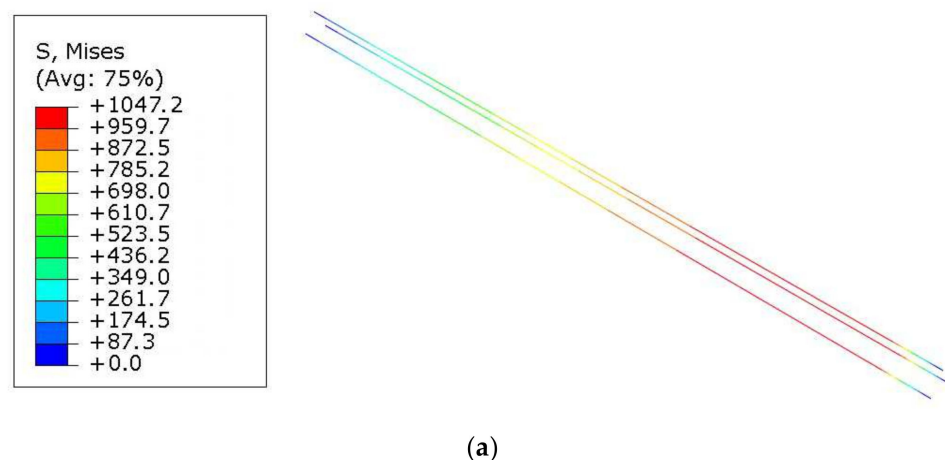


**Figure 12. Cont.**

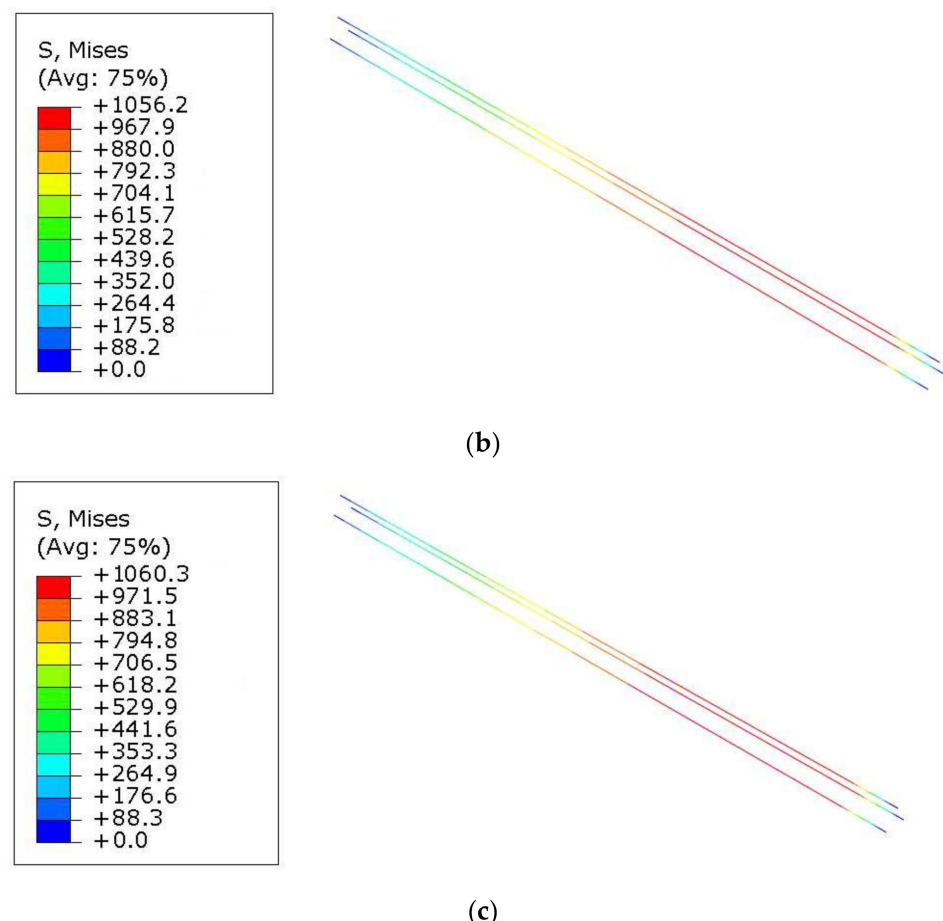


**Figure 12.** Stress distribution in prestressed steel wire strand at end anchoring failure on one side of (MPa): (a) S3; (b) S1; (c) S4.

The confinement effect of stirrups on concrete can effectively improve the ultimate compressive strength of concrete and delay the occurrence of splitting cracks. This improves the bond strength between the concrete and steel strands, thereby reducing the secondary transfer length of residual prestress. The initial effective pre-tension of S1, S5, and S6 are set as 497 kN for the corrosion test simulation. The stress distribution of reinforcement cages with different diameters when the end anchoring of one side of the specimen fails are shown in Figure 13. As indicated, although S1 reaches the maximum stress value of 77.6 MPa among these three specimens, this value is still at a low stress level. This means that the confinement of the stirrup on the concrete is relatively small, and the effect of the stirrup on the secondary transfer of residual prestress is not significant. In other words, the stirrups do not fully exert their confinement effect in this case. Therefore, increasing the diameter of stirrups has no significant effect on the secondary transfer length before the splitting cracks appear in the concrete.

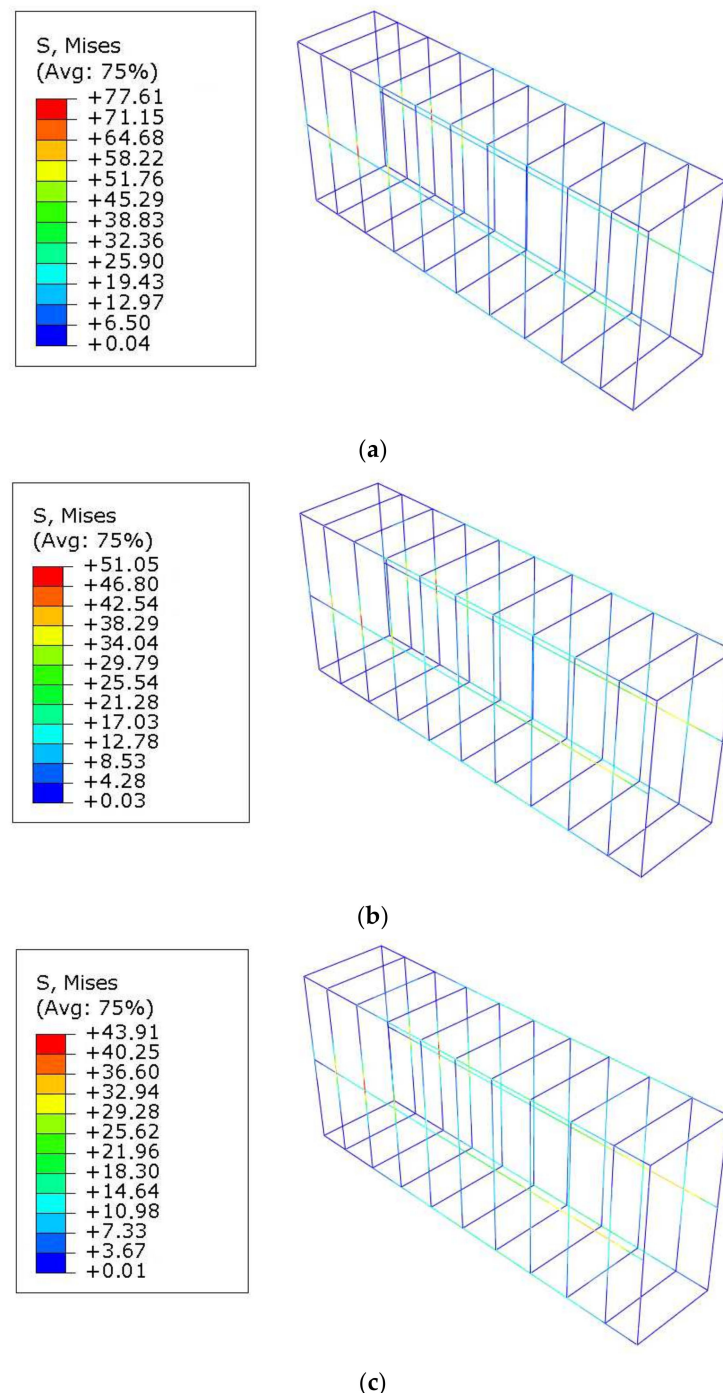


**Figure 13.** Stress distribution of reinforcement cage at end anchoring failure of one side (MPa): (a) S1; (b) S5; (c) S6.

According to the definition of secondary transfer, the secondary transfer length, which is calculated in the numerical simulation, is shown in Table 5. The numerical simulation results have a small error with the test results. The average error of all specimens is only 2.62%, and the maximum error is only 5.2%. Hence, the proposed numerical simulation method has high accuracy.

**Table 5.** Secondary transfer length of S1–S6 in the numerical simulation.

Specimens No.	Concrete Comprehensive Strength/MPa	Concrete Tensile Strength/(MPa)	Tensile Force of Steel Wire Strand in the Beginning of Corrosion/kN	Transfer Length in Equation (5) $l_{t1}/\text{mm}$	Transfer Length in Numerical Simulation $l_{t3}/\text{mm}$	Relative Error/%
S1	53.5	3.69	497.2	655	675	3.1
S2	53.5	3.69	511.3	673	680	1.0
S3	42.6	3.34	449.9	664	690	3.9
S4	63.3	4.13	510.5	618	650	5.2
S5	53.5	3.69	501.1	660	670	1.5
S6	53.5	3.69	505.2	665	670	0.8

## 5. Conclusions

The secondary transfer behaviors of residual prestress after corrosion and fracture failure at the anchoring end on one side of six different post-tensioning prestressed concrete specimens were studied through an experiment in this study. The influences of concrete strength, stirrup configuration, and length of components on the secondary transfer of prestress and anchoring performances were analyzed. The calculation method of the secondary transfer of residual prestress was discussed preliminarily. Some major conclusions can be drawn:

- (1) After the corrosion fracture of the steel wire strand at the end anchoring, shrinkage and slippage occurred in the stranded wire. Due to the bonding action between the concrete and the strands, the strain of the steel wire strand on the corrosion side of all specimens decreases quickly, and the strain changes within a certain length range are close to zero. Similar to the pre-tensioning method, the residual prestress of the steel wire strand at the end of the corrosion fracture process can realize effective secondary transfer within a certain range when it has good bonding performance with concrete.
- (2) Although residual prestress can undergo a secondary transfer after the corrosion fracture of the steel wire strand, effective prestress will decrease in all specimens. The loss ratio of prestress is negatively related to concrete strength. The lower the concrete strength, the higher the loss ratio of prestress. The stirrup diameter can slightly influence the effective prestress after transfer.
- (3) The secondary transfer length of residual prestress is significantly correlated with concrete tensile strength. A higher concrete strength leads to a smaller secondary transfer length. When the thickness of the protective cover exceeds five times the diameter of prestressed tendons, the structure develops no splitting failure. Stirrup area changes influence the secondary transfer length slightly.
- (4) Whether secondary transfer after the corrosion fracture of steel wire strand is determined by their bond performances. In the existing standards, the calculation of the secondary transfer length of residual prestress in the steel wire strand is too conservative and safe. The calculation method of the secondary transfer length based on the principle of equal actual stress and bond force of steel wire strands has a relatively high calculation accuracy. The average error and maximum error are only 2.58% and 5.2%, respectively.
- (5) The post-tensioning components have relatively small sizes in this study, which will bring greater losses of prestress. Hence, secondary transfer performances of prestress based on actual bridge size components have to be further studied. Additionally, reliability evaluation and prediction of existing bridges also have to be further studied with considerations made to the types of corrugated pipes used and the loosening of the steel wire strands.

The limitation of this study is that only the secondary transfer of residual prestress of short specimens is considered, and the transfer law of longer specimens needs to be further studied.

**Author Contributions:** Conceptualization, R.Y.; methodology, R.Y., X.Z. and X.W.; software, R.Y.; validation, R.Y. and Y.Y.; writing—original draft preparation, R.Y. and Y.Y.; writing—review and editing, R.Y., Y.Y., X.Z. and X.W.; supervision, X.Z. and X.W.; funding acquisition, R.Y., Y.Y. and X.W. All authors have read and agreed to the published version of the manuscript.

**Funding:** This research was funded by the National Natural Science Foundation of China (Grant No. 52208166), the Science and Technology Innovation Program of Hunan Province (2022RC1186), the Hunan Provincial Natural Science Foundation of China (grant no. 2021JJ50156, 2022JJ40024, and 2021JJ50153), the Research Foundation of Education Bureau of Hunan Province (grant no. 21B0723), the Open Fund of Key Laboratory of Safety Control of Bridge Engineering, Ministry of Education (Changsha University of Science & Technology) (21KB03), the Open Project of State Key Laboratory of Performance Monitoring and Protecting of Rail Transit Infrastructure (East China Jiaotong University) (HJGZ2022108), and the Aid program for Science and Technology Innovative Research Team in Higher Educational Institutions of Hunan Province.

**Data Availability Statement:** Not applicable.

**Acknowledgments:** We would like to thank the anonymous reviewers and the editor for their valuable comments and remarks that helped us to improve the original manuscript.

**Conflicts of Interest:** The authors declare no conflict of interest.

## References

1. Charles, W.D.; Hamilton, H.R. *Prestressed Concrete: Building, Design, and Construction*; Springer: Berlin/Heidelberg, Germany, 2019.
2. Yang, Y.M.; Peng, J.X.; Liu, X.H.; Cai, S.C.S.; Zhang, J.R. Probability analysis of web cracking of corroded prestressed concrete box-girder bridges considering aleatory and epistemic uncertainties. *Eng. Struct.* **2021**, *228*, 111486. [[CrossRef](#)]
3. Yang, Y.M.; Liu, Z.H.; Tang, H.; Peng, J.X. Deflection-based failure probability analysis of low shrinkage-creep concrete structures in presence of non-stationary evolution of shrinkage and creep uncertainties. *Constr. Build. Mater.* **2023**, *376*, 131077. [[CrossRef](#)]
4. Yang, Y.M.; Peng, J.X.; Cai, C.S.; Zhou, Y.D.; Wang, L.; Zhang, J.R. Time-dependent reliability assessment of aging structures considering stochastic resistance degradation process. *Reliab. Eng. Syst. Saf.* **2022**, *217*, 108105. [[CrossRef](#)]
5. Ye, J. *Principles of Structural Design*; China Communications Press Co., Ltd.: Beijing, China, 2019.
6. Yang, J.M.; Kim, J.K.; Yoo, D.Y. Transfer length in full-scale pretensioned concrete beams with 1.4 m and 2.4 m section depths. *Eng. Struct.* **2018**, *171*, 433–444. [[CrossRef](#)]
7. Ramirez-Garcia, A.T.; Dang, C.N.; Hale, W.M. A higher-order equation for modeling strand bond in pretensioned concrete beams. *Eng. Struct.* **2017**, *131*, 345–361. [[CrossRef](#)]
8. Martí-Vargas, J.; Caro, L.A.; Serna, P. Experimental Technique for Measuring the Long-term Transfer Length in Prestressed Concrete. *Strain* **2013**, *49*, 125–134. [[CrossRef](#)]
9. ACI Committee. *Building Code Requirements for Structural Concrete (ACI 318-08) and Commentary*; American Concrete Institute: Farmington Hills, MI, USA, 2014.
10. American Association of State Highway and Transportation Officials. *Standard Specifications for Highway Bridges*; Aashto: Washington, DC, USA, 2002.
11. Hendy, C.R.; Johnson, R.; Gulvanessian, H. *Eurocode 4-Design of Composite Steel and Concrete Structures—Part 2: General Rules and Rules for Bridges*; European Commission: Brussels, Belgium, 2006.
12. GB 50010-2020; Code for Design of Concrete Structures. China Architecture and Building Press: Beijing, China, 2020.
13. Almohammed, A.; Kareem, R.S.; Dang, C.N.; Martí-Vargas, J.R.; Hale, W.M. Analytical model for predicting prestress transfer bond-related parameters of 18 mm prestressing strands. *J. Build. Eng.* **2022**, *56*, 104709. [[CrossRef](#)]
14. Motwani, P.; Laskar, A. Influence of excessive end slippage on transfer length of prestressing strands in PC members. *Structures* **2019**, *20*, 676–688. [[CrossRef](#)]
15. Al-Kaimakchi, A.; Rambo-Roddenberry, M. Measured transfer length of 15.2-mm (0.6-in.) duplex high-strength stainless steel strands in pretensioned girders. *Eng. Struct.* **2021**, *237*, 112178. [[CrossRef](#)]
16. Motwani, P.; Rather, A.I.; Laskar, A. Transfer stage parameters for concrete beams prestressed with BFRP bars: Experimental and finite element studies. *Constr. Build. Mater.* **2022**, *315*, 125639. [[CrossRef](#)]
17. Anaya, P.; Martín-Pérez, P.; Rodríguez, J.; Andrade, C. Transfer length of corroded wires in prestressed concrete members. *Struct. Concr.* **2022**, *23*, 154–171. [[CrossRef](#)]
18. Jokubaitis, A.; Valivonis, J. An analysis of the transfer lengths of different types of prestressed fiber-reinforced polymer reinforcement. *Polymers* **2022**, *14*, 3931. [[CrossRef](#)] [[PubMed](#)]
19. Alkurdi, Z. Influence of concrete compressive strength on transfer length in pretensioned concrete members using 3D Nonlinear FEM Analysis. In Proceedings of the 6th International Conference on Civil, Structural and Transportation Engineering (ICCSTE'21), Niagara Falls, ON, Canada, 17–19 May 2021.
20. Arezoumandi, M.; Looney, K.B.; Volz, J.S. An experimental study on transfer length of prestressing strand in self-consolidating concrete. *Eng. Struct.* **2020**, *208*, 110317. [[CrossRef](#)]

21. Lan, G.H.; Wang, C.D.; Chen, H.; Zhao, W.W. Experimental study on transfer length of prestressing strands in Ningju intercity rail transit U-beams. *Build. Struct.* **2022**, *52*, 5.
22. Abdelatif, A.O.; Owen, J.S.; Hussein, M.F.M. Modelling the prestress transfer in pre-tensioned concrete elements. *Finite Elem. Anal. Des.* **2015**, *94*, 47–63. [[CrossRef](#)]
23. Dai, L.Z.; Chen, H.; Wang, L.; Ma, Y.F.; Zhang, J.R. Transfer length prediction in pre-tensioned concrete beams under corrosive cracking. *Structures* **2021**, *30*, 938–948. [[CrossRef](#)]
24. Wang, L.; Zhang, X.H.; Zhang, J.R.; Ma, Y.F.; Xiang, Y.B.; Liu, Y.M. Effect of insufficient grouting and strand corrosion on flexural behavior of PC beams. *Constr. Build. Mater.* **2014**, *53*, 213–224. [[CrossRef](#)]
25. Alhassan, M.A.; Ababneh, A.N.; Betoush, N.A. Innovative model for accurate prediction of the transfer length of prestressing strands based on artificial neural networks: Case study. *Case Stud. Constr. Mater.* **2020**, *12*, e00312. [[CrossRef](#)]
26. Zghayar, E.E.; Mackie, K.R.; Haber, Z.B.; Potter, W. Secondary anchorage in post-tensioned bridge systems. *ACI Struct. J.* **2013**, *110*, 629–638.
27. Dai, L.Z.; Chen, Y.; Wang, L.; Ma, Y.F. Secondary anchorage and residual prestressing force in locally corroded PT beams after strand fracture. *Constr. Build. Mater.* **2021**, *275*, 122137. [[CrossRef](#)]
28. Yang, R.H.; Zhang, J.R.; Wang, L.; Zhang, X.H. Experimental research for flexural behavior on concrete beams with local corrosion fracture of strands. *J. Cent. South Univ. (Sci. Technol.)* **2018**, *49*, 9.
29. Belarbi, A.; Hsu, T. Constitutive laws of concrete in tension and reinforcing bars stiffened by concrete. *ACI Struct. J.* **1994**, *91*, 465–474.
30. Yang, R.; Yang, Y.M.; Zhang, X.H.; Wang, X.Z. Experimental study on performance of local bond-slip test of steel strand tendons and concrete. *Coatings* **2022**, *12*, 1494. [[CrossRef](#)]
31. Wang, Y. *Abaqus Analysis User's Guide: Material*; China Machine Press: Beijing, China, 2021.

**Disclaimer/Publisher's Note:** The statements, opinions and data contained in all publications are solely those of the individual author(s) and contributor(s) and not of MDPI and/or the editor(s). MDPI and/or the editor(s) disclaim responsibility for any injury to people or property resulting from any ideas, methods, instructions or products referred to in the content.